

# SUPPLEMENTARY MATERIAL FOR “DISCONTINUOUS GALERKIN METHODS FOR THE VLASOV-MAXWELL EQUATIONS”

YINGDA CHENG\*, IRENE M. GAMBA†, FENGYAN LI‡, AND PHILIP J. MORRISON§

This file contains supplementary figures to the paper “Discontinuous Galerkin Methods for the Vlasov-Maxwell Equations”.

Figures S1 to S5 are for parameter choice 1 as in Califano *et al.* [1]. In Figure S1, we study the effect of enlarging the domain in the velocity direction. The growth in the total mass, as time approaches  $T = 200$  when  $\Omega_\xi = [-1.2, 1.2]^2$ , implies that up to this time, a larger domain should be used in order for the assumption,  $f$  being compactly supported in  $\xi$ , to still hold. This growth in relative error is not observed when  $\Omega_\xi = [-1.5, 1.5]^2$ . On the other hand, the decay in the total energy with the upwind fluxes is largely due to the tangential jump terms in the electric and magnetic field as derived in Lemma 3.2. Therefore, enlarging the domain has little effects on this. As for the decay in total energy with central and alternating fluxes, we can see that enlarging the domain roughly reduces the error by half. The other part of the error is coming from the dissipative nature of the TVD-RK scheme that we have used. In Figure S2, we plot the evolution of the density at various times as indicated. In Figures S3 and S4 we plot the 2D contours of  $f$  at selected locations  $x_2$  and time  $t$ , when the upwind flux is used in the Maxwell solver. The times chosen correspond to those for the density of Figure S2, and we see that at late times considerable fine structure is present, which is consistent with the Log Fourier plots. For completeness, we also include in Figure S5 plots of the electric and magnetic fields at the final time for our three fluxes.

Figures S6 to S10 are for nonsymmetric parameter set, choice 2 of the Califano paper. Again we observe relatively larger error in the total energy when the upwind flux is used to solve Maxwell’s equations. But overall, both mass and total energy are very well preserved. Insofar as we can make comparison with [1], our results are in reasonable agreement. Similar energy transfers take place, but the equipartition of the magnetic and electric energies at the peak is not achieved. All modes saturate now at nearly the same values, evidently resulting from the broken symmetry. Also, at long times, contours of the distribution function are displayed. Here the wrapping of the distribution function as two intertwined distorted cylinders is observed as in [1], although for late times there is a loss of localization.

## REFERENCES

- [1] F. Califano, F. Pegoraro, S. V. Bulanov, and A. Mangeney. Kinetic saturation of the Weibel instability in a collisionless plasma. *Phys. Rev. E*, 57(6):7048–7059, 1998.

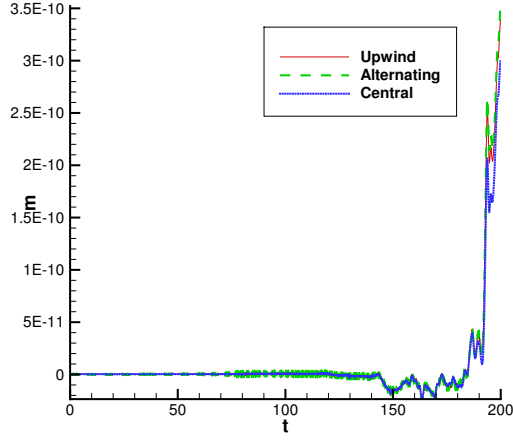
---

\*Department of Mathematics, Michigan State University, East Lansing, MI 48824 U.S.A. [ycheng@math.msu.edu](mailto:ycheng@math.msu.edu)

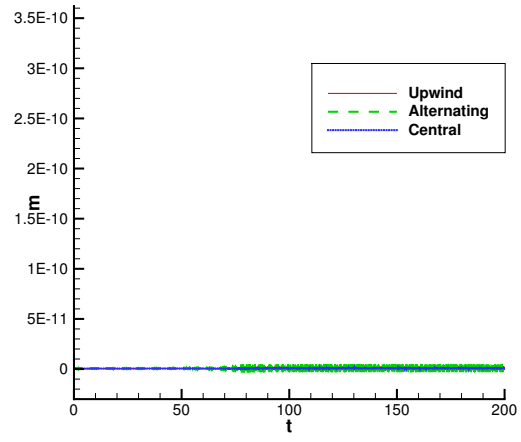
†Department of Mathematics and ICES, University of Texas at Austin, Austin, TX 78712 U.S.A. [gamba@math.utexas.edu](mailto:gamba@math.utexas.edu)

‡Department of Mathematical Sciences, Rensselaer Polytechnic Institute, Troy, NY 12180, U.S.A. [lif@rpi.edu](mailto:lif@rpi.edu)

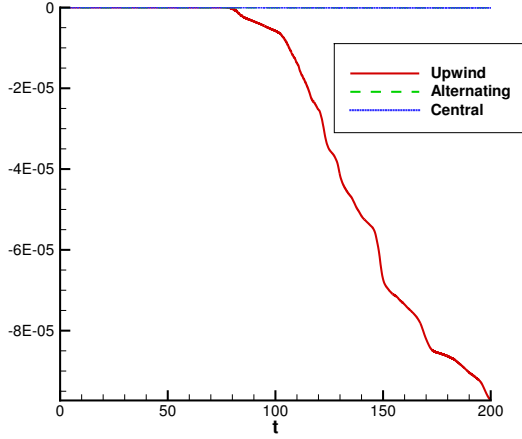
§Department of Physics and Institute for Fusion Studies, University of Texas at Austin, Austin, TX 78712 U.S.A. [morrison@physics.utexas.edu](mailto:morrison@physics.utexas.edu)



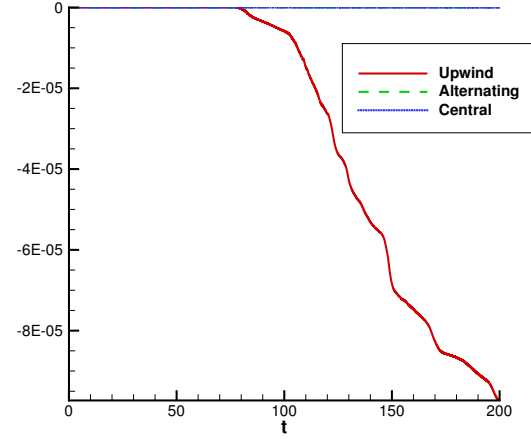
(a) Relative error for mass with small domain



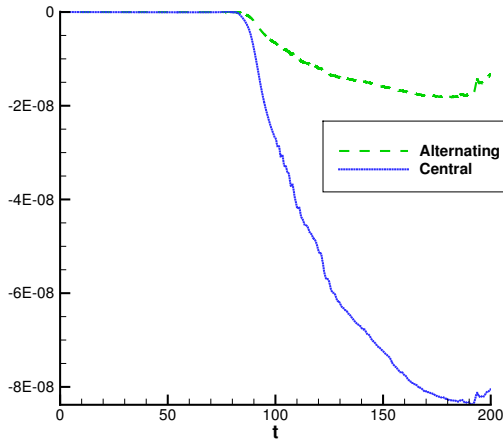
(b) Relative error for mass with large domain



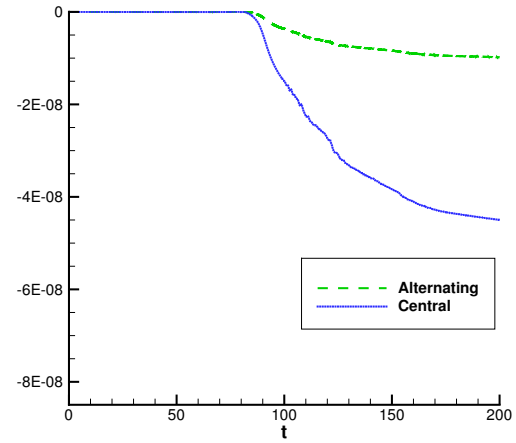
(c) Relative error for total energy with small domain



(d) Relative error for total energy with large domain

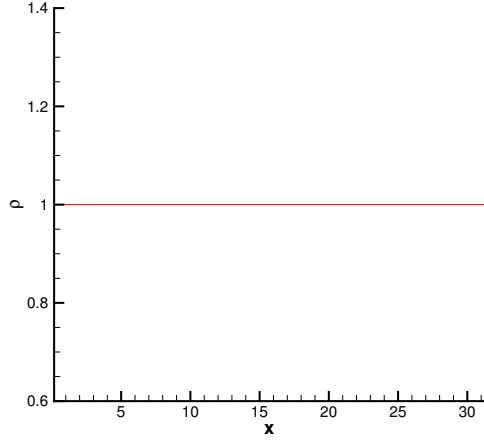


(e) Relative error for total energy of central and alternating fluxes with small domain

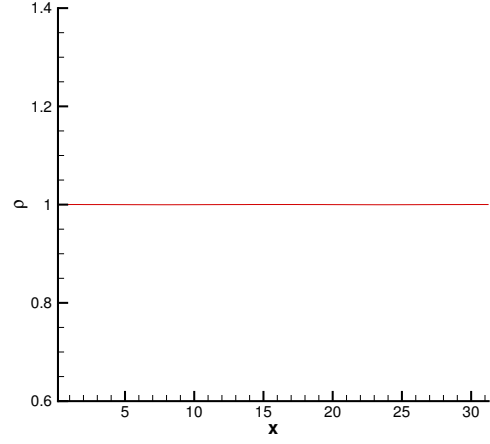


(f) Relative error for total energy of central and alternating fluxes with large domain

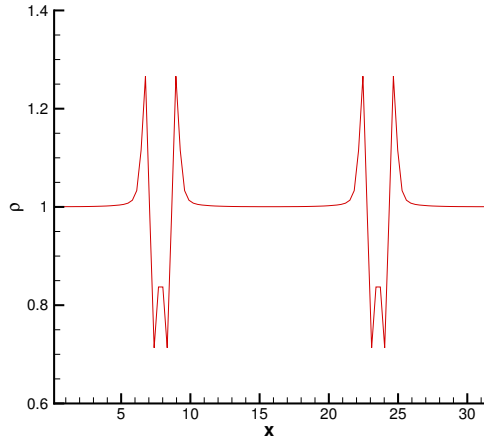
FIG. S1. Streaming Weibel instability with parameter choice 1 as in Califano et al. [1] ( $\delta = 0.5$ ,  $v_{0,1} = v_{0,2} = 0.3$ ,  $k_0 = 0.2$ ), the symmetric case. Effects of enlarging the domain. The runs are conducted on the same mesh size, but with different domains in the velocity space. The small domain is  $\Omega_\xi = [-1.2, 1.2]^2$ , the large domain is  $\Omega_\xi = [-1.5, 1.5]^2$



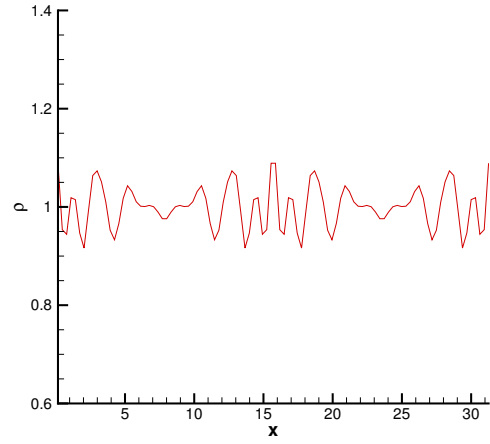
(a)  $t = 0$ .



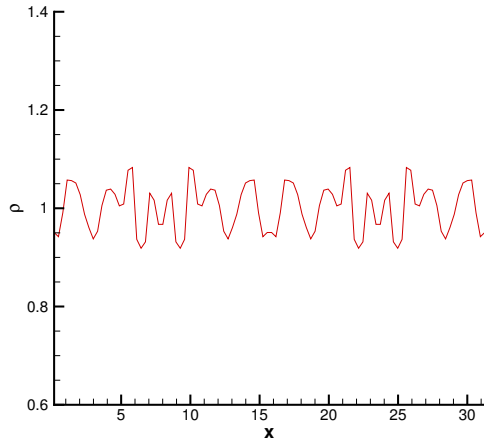
(b)  $t = 55$ .



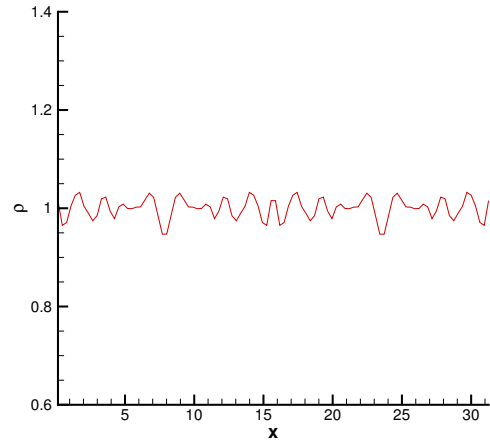
(c)  $t = 82$ .



(d)  $t = 100$ .

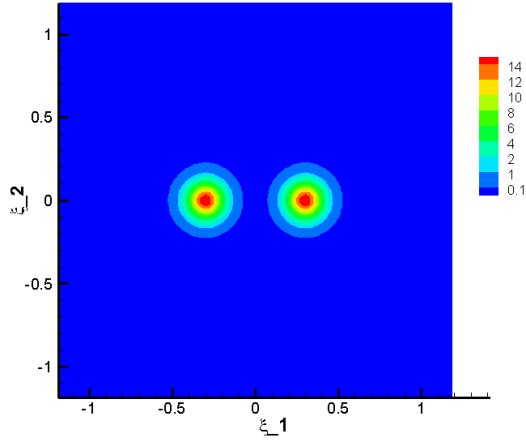


(e)  $t = 125$ .

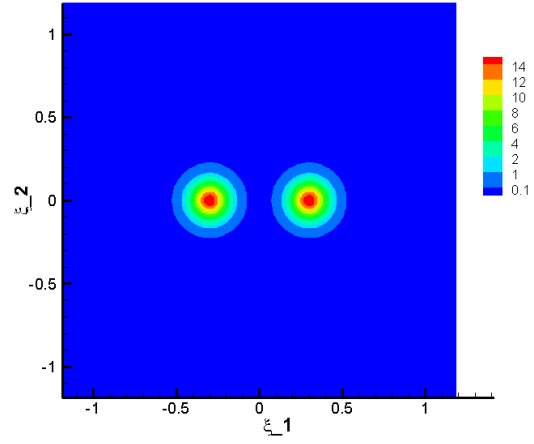


(f)  $t = 175$ .

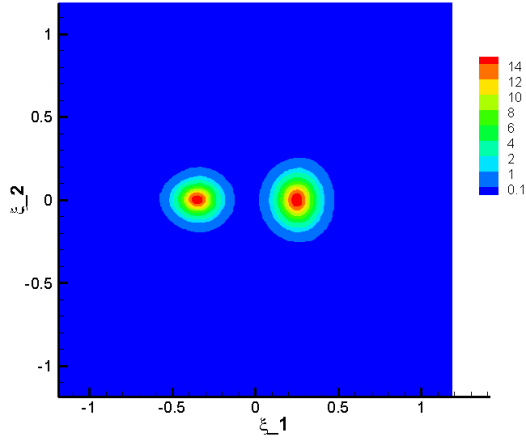
FIG. S2. Plots of the computed density function  $\rho_h$  for the streaming Weibel instability, with parameter choice 1 as in [1] ( $\delta = 0.5, v_{0,1} = v_{0,2} = 0.3, k_0 = 0.2$ ), at selected time  $t$ . The mesh is  $100^3$  with piecewise quadratic polynomials. The upwind flux is applied.



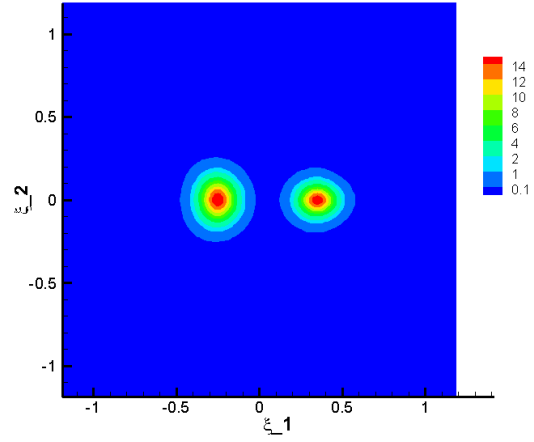
(a)  $x_2 = 0.05\pi$ ,  $t = 0$ .



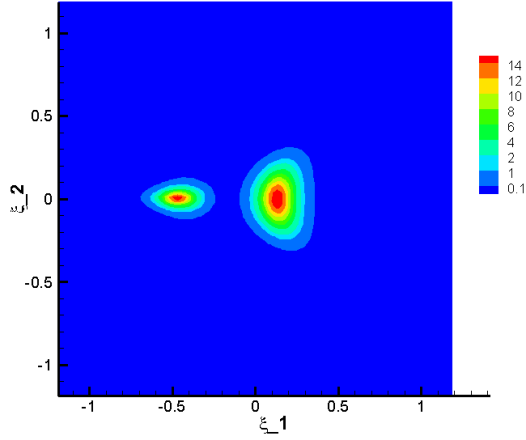
(b)  $x_2 = 4.95\pi$ ,  $t = 0$ .



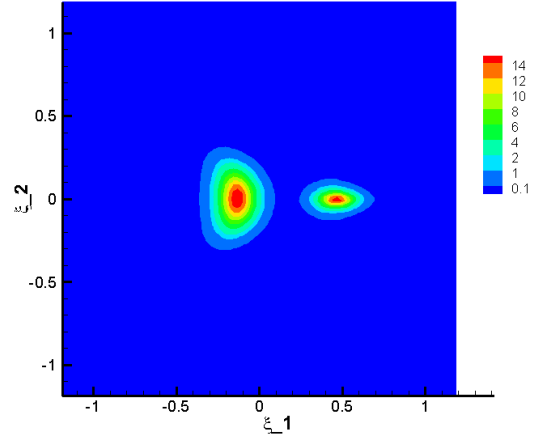
(c)  $x_2 = 0.05\pi$ ,  $t = 55$ .



(d)  $x_2 = 4.95\pi$ ,  $t = 55$ .

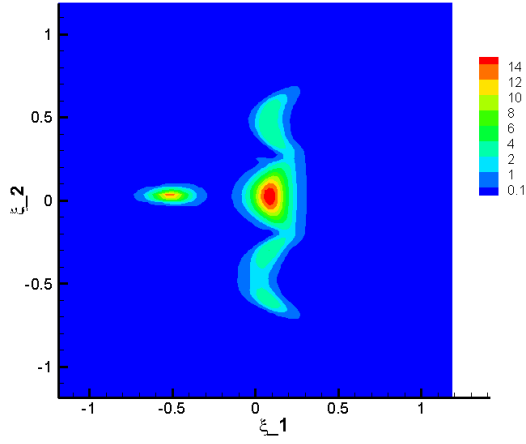


(e)  $x_2 = 0.05\pi$ ,  $t = 82$ .

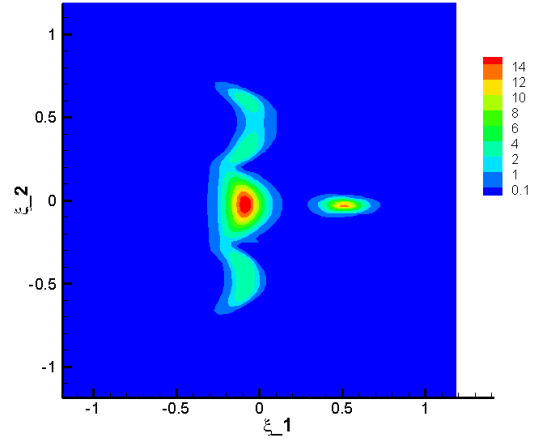


(f)  $x_2 = 4.95\pi$ ,  $t = 82$ .

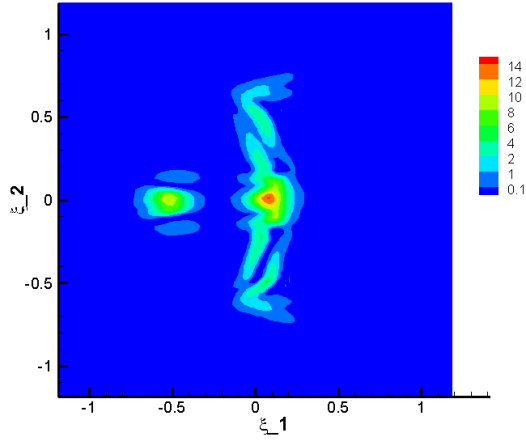
FIG. S3. 2D contour plots of the computed distribution function  $f_h$  for the streaming Weibel instability, with parameter choice 1 as in [1] ( $\delta = 0.5, v_{0,1} = v_{0,2} = 0.3, k_0 = 0.2$ ), at selected location  $x_2$  and time  $t$ . The mesh is  $100^3$  with piecewise quadratic polynomials. The upwind flux is applied.



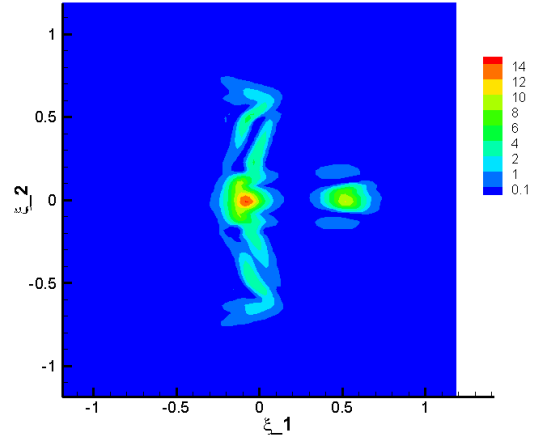
(a)  $x_2 = 0.05\pi$ ,  $t = 100$ .



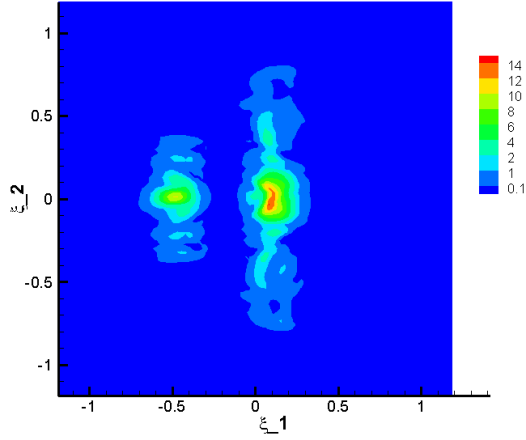
(b)  $x_2 = 4.95\pi$ ,  $t = 100$ .



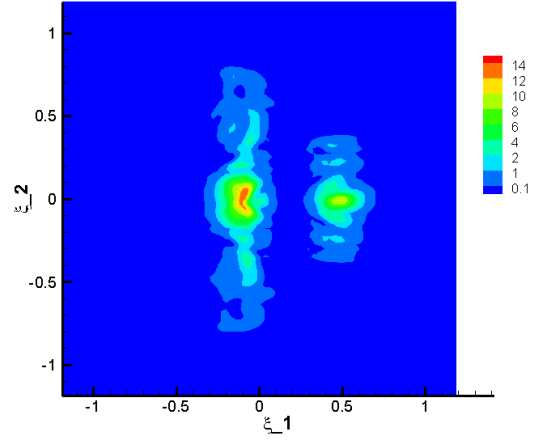
(c)  $x_2 = 0.05\pi$ ,  $t = 125$ .



(d)  $x_2 = 4.95\pi$ ,  $t = 125$ .

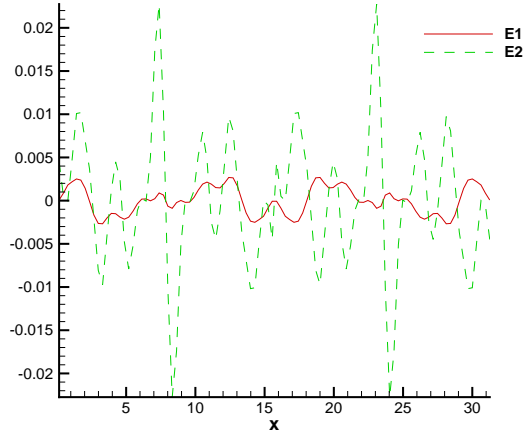


(e)  $x_2 = 0.05\pi$ ,  $t = 175$ .

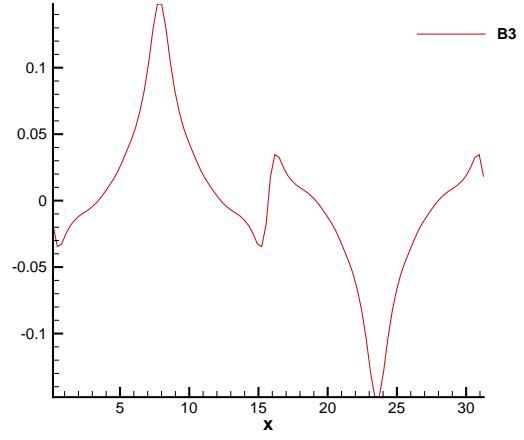


(f)  $x_2 = 4.95\pi$ ,  $t = 175$ .

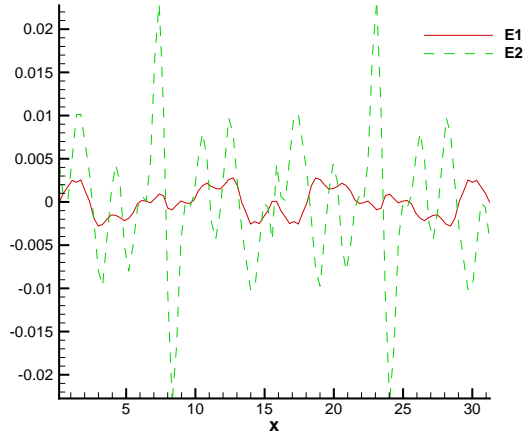
FIG. S4. 2D contour plots of the computed distribution function  $f_h$  for the streaming Weibel instability, with parameter choice 1 as in [1] ( $\delta = 0.5, v_{0,1} = v_{0,2} = 0.3, k_0 = 0.2$ ), at selected location  $x_2$  and time  $t$ . The mesh is  $100^3$  with piecewise quadratic polynomials. The upwind flux is applied.



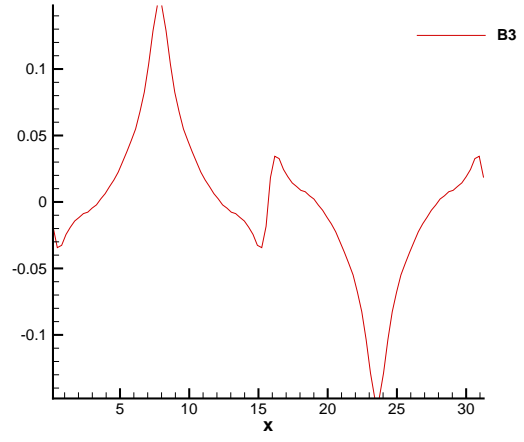
(a) Electric field, upwind flux



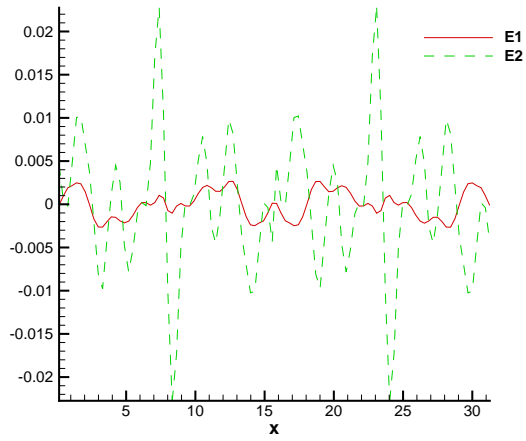
(b) Magnetic field, upwind flux



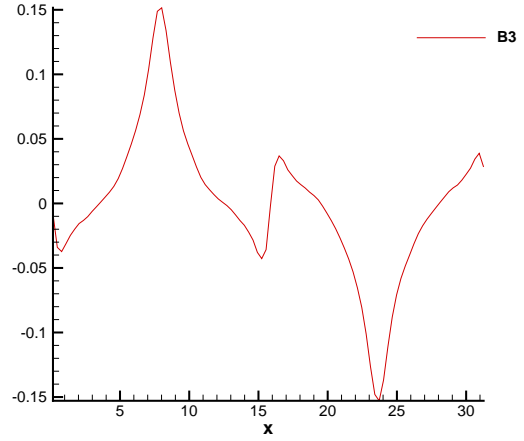
(c) Electric field, central flux



(d) Magnetic field, central flux



(e) Electric field, alternating flux



(f) Magnetic field, alternating flux

FIG. S5. Streaming Weibel instability with parameter choice 1 as in [1] ( $\delta = 0.5, v_{0,1} = v_{0,2} = 0.3, k_0 = 0.2$ ). The mesh is  $100^3$  with piecewise quadratic polynomials. The electric and magnetic fields at  $T = 200$ .

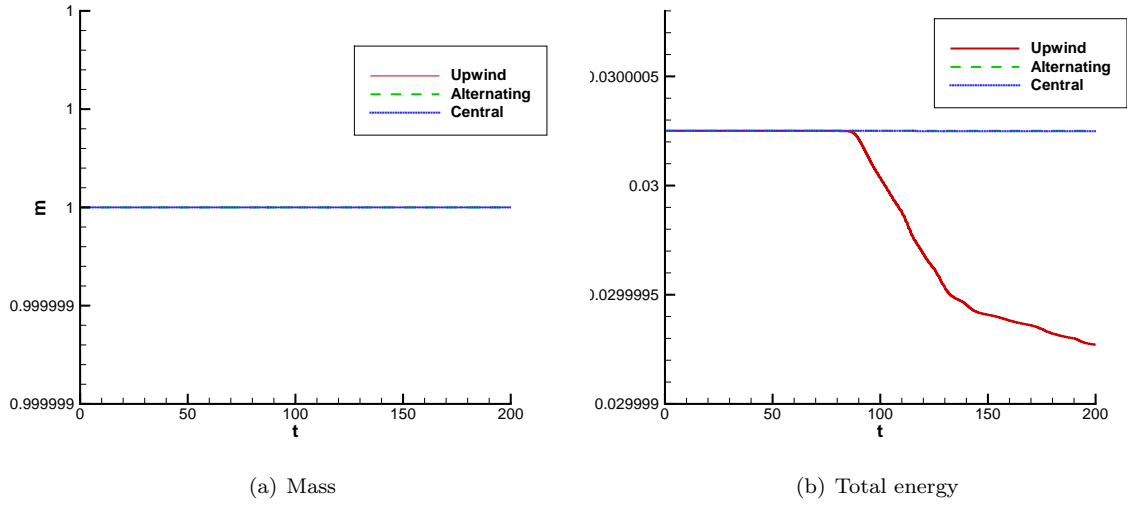
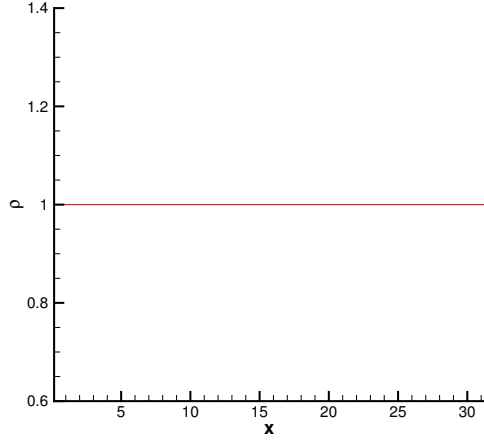
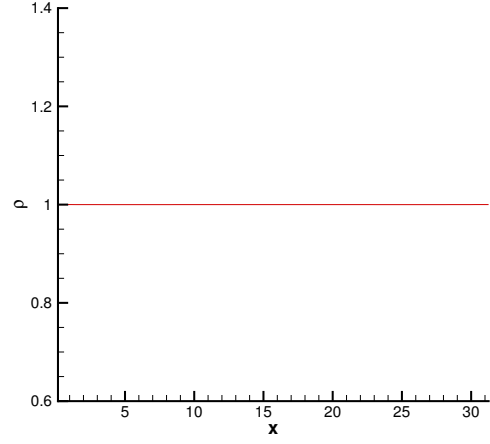


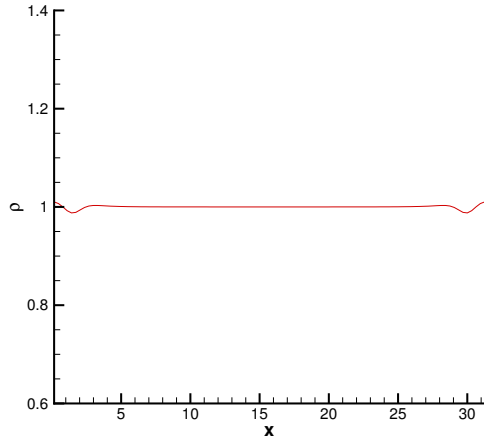
FIG. S6. Streaming Weibel instability with parameter choice 2 as in Califano et al. [1] ( $\delta = 1/6$ ,  $v_{0,1} = 0.5$ ,  $v_{0,2} = 0.1$ ,  $k_0 = 0.2$ ), the non-symmetric case. The mesh is  $100^3$  with piecewise quadratic polynomials. Time evolution of mass, total energy with three numerical fluxes for the Maxwell's equations.



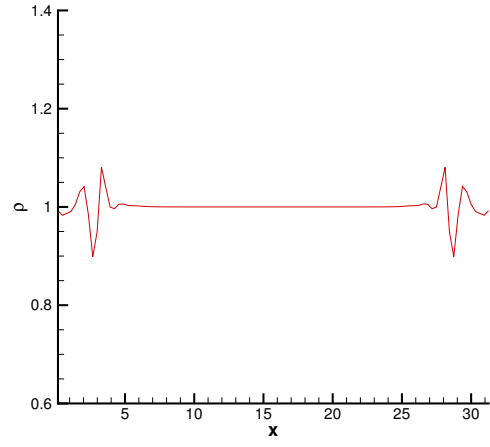
(a)  $t = 0$ .



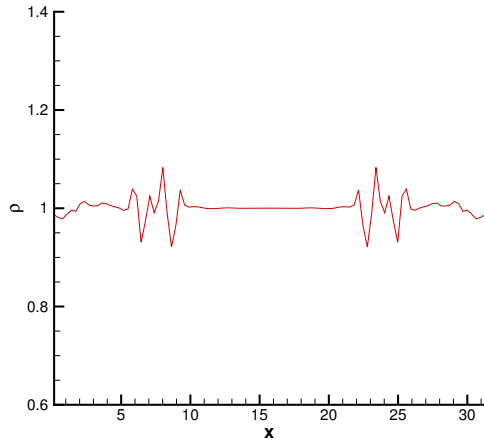
(b)  $t = 55$ .



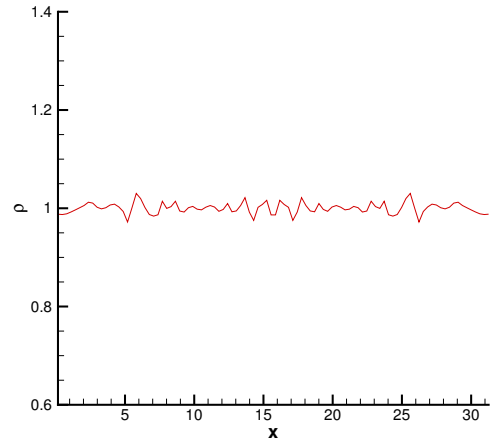
(c)  $t = 82$ .



(d)  $t = 100$ .



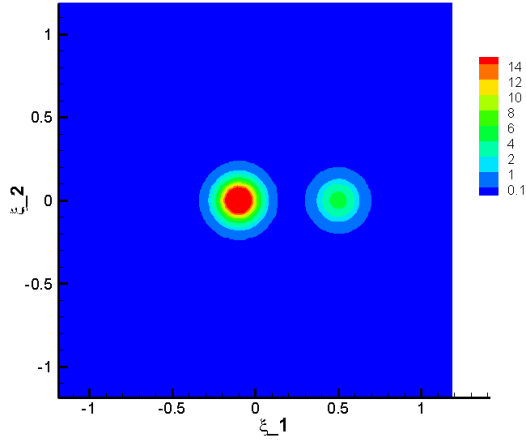
(e)  $t = 125$ .



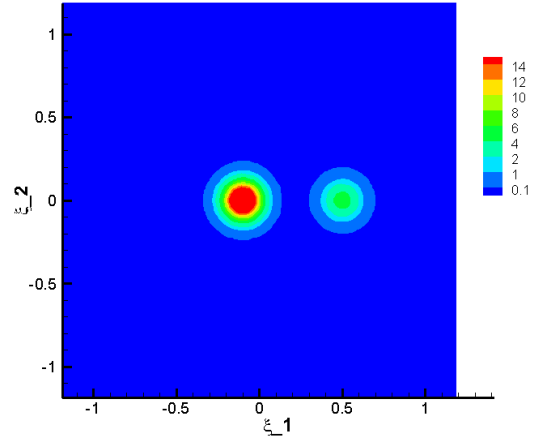
(f)  $t = 175$ .

FIG. S7. Plots of the computed density function  $\rho_h$  for the streaming Weibel instability, with parameter choice 2 as in [1] ( $\delta = 1/6, v_{0,1} = 0.5, v_{0,2} = 0.1, k_0 = 0.2$ ), at selected times. The mesh is  $100^3$  with piecewise quadratic polynomials. The upwind flux is applied.

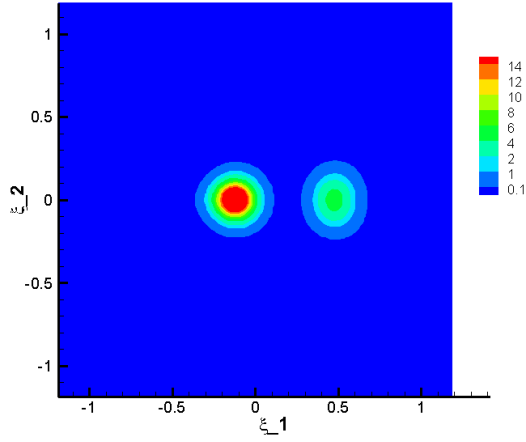




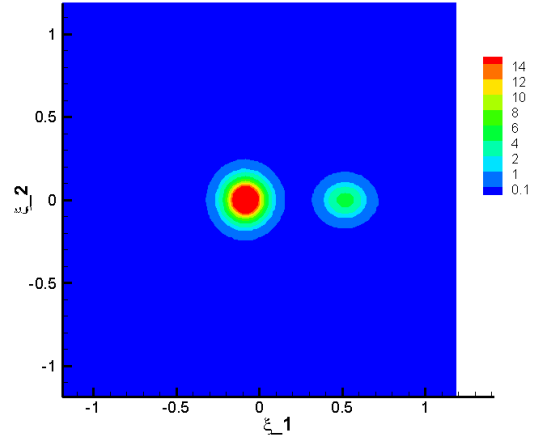
(a)  $x_2 = 0.05\pi$ ,  $t = 0$ .



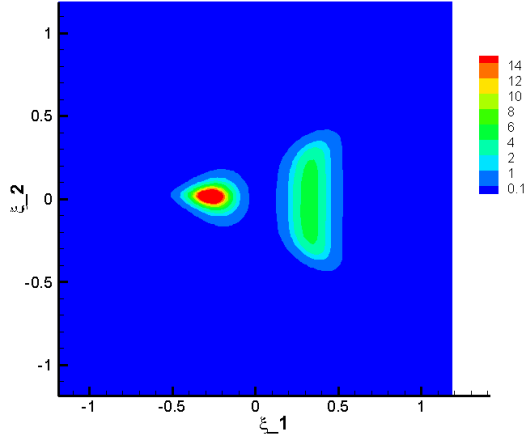
(b)  $x_2 = 4.95\pi$ ,  $t = 0$ .



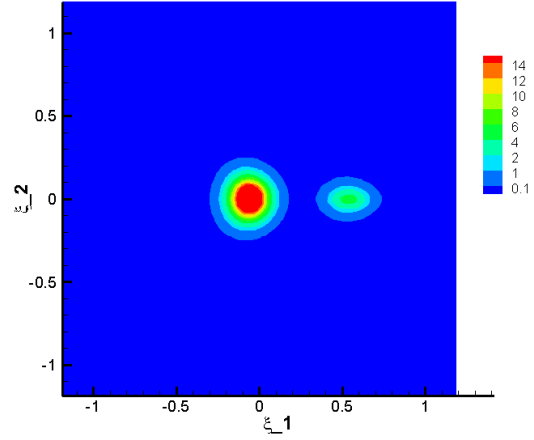
(c)  $x_2 = 0.05\pi$ ,  $t = 55$ .



(d)  $x_2 = 4.95\pi$ ,  $t = 55$ .

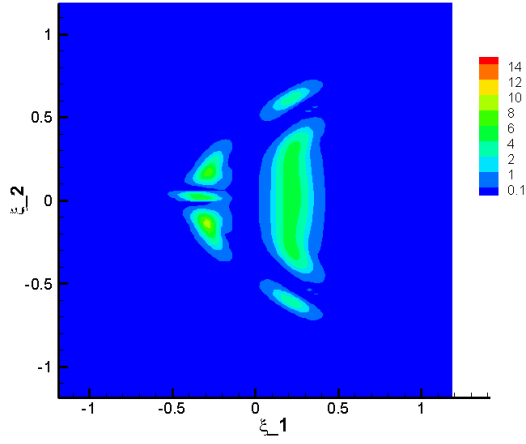


(e)  $x_2 = 0.05\pi$ ,  $t = 82$ .

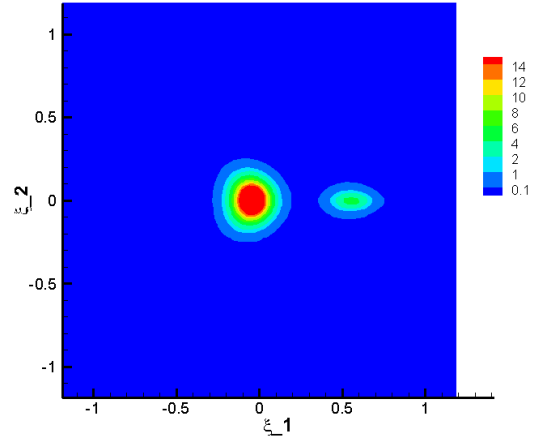


(f)  $x_2 = 4.95\pi$ ,  $t = 82$ .

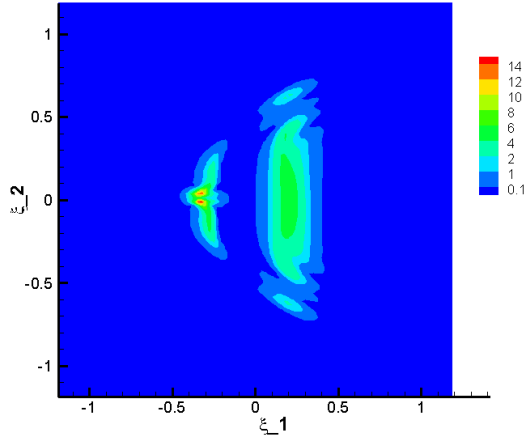
FIG. S8. 2D contour plots of the computed distribution function  $f_h$  for the streaming Weibel instability, with parameter choice 2 as in [1] ( $\delta = 1/6$ ,  $v_{0,1} = 0.5$ ,  $v_{0,2} = 0.1$ ,  $k_0 = 0.2$ ), at selected location  $x_2$  and time  $t$ . The mesh is  $100^3$  with piecewise quadratic polynomials. The upwind flux is applied.



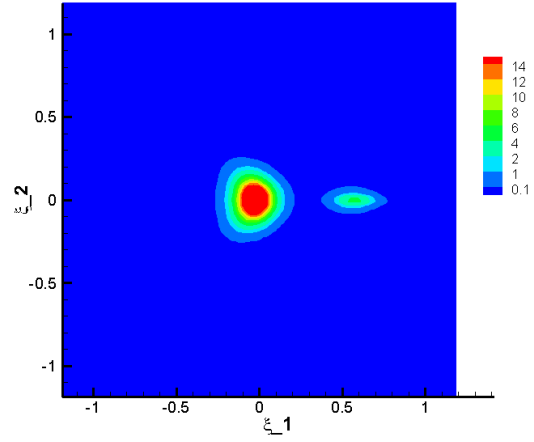
(a)  $x_2 = 0.05\pi$ ,  $t = 100$ .



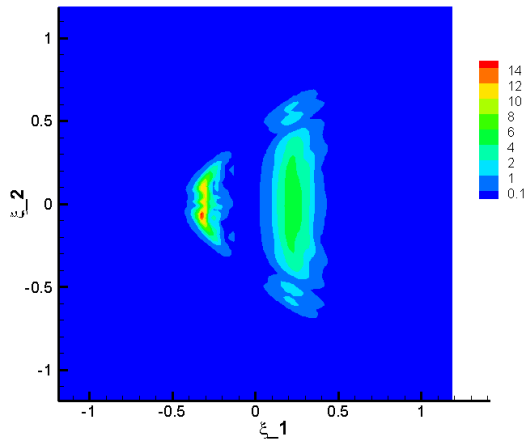
(b)  $x_2 = 4.95\pi$ ,  $t = 100$ .



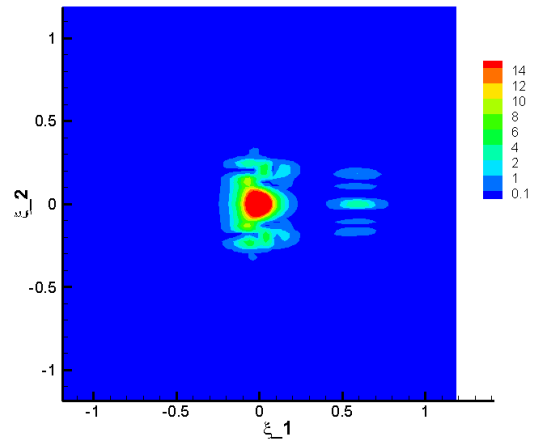
(c)  $x_2 = 0.05\pi$ ,  $t = 125$ .



(d)  $x_2 = 4.95\pi$ ,  $t = 125$ .

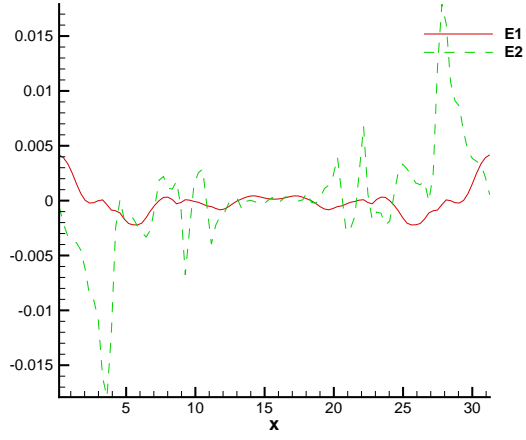


(e)  $x_2 = 0.05\pi$ ,  $t = 175$ .

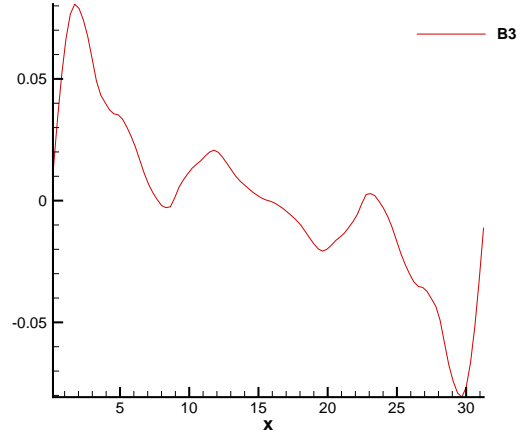


(f)  $x_2 = 4.95\pi$ ,  $t = 175$ .

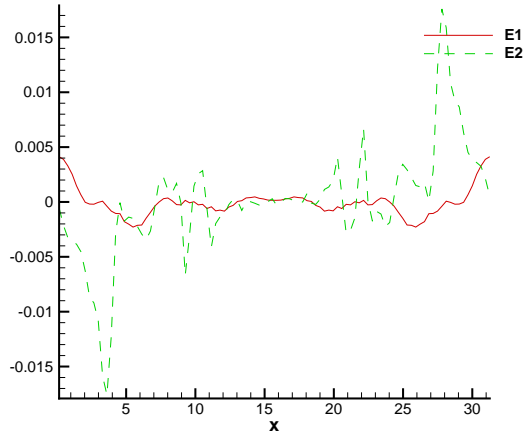
FIG. S9. 2D contour plots of the computed distribution function  $f_h$  for the streaming Weibel instability, with parameter choice 2 as in [1] ( $\delta = 1/6$ ,  $v_{0,1} = 0.5$ ,  $v_{0,2} = 0.1$ ,  $k_0 = 0.2$ ), at selected location  $x_2$  and time  $t$ . The mesh is  $100^3$  with piecewise quadratic polynomials. The upwind flux is applied.



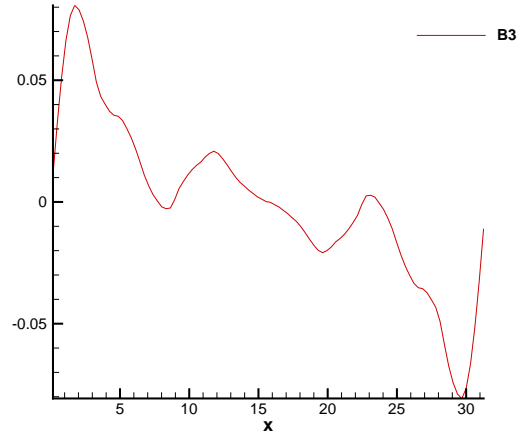
(a) Electric field, upwind flux



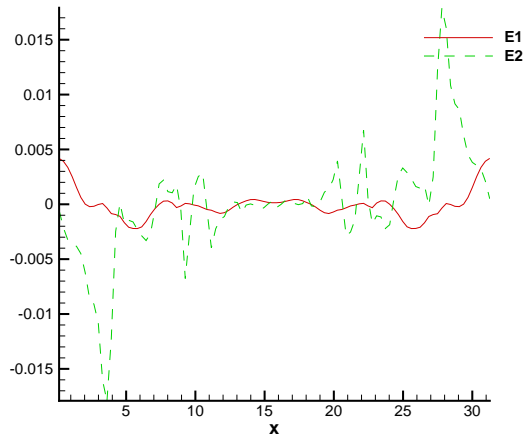
(b) Magnetic field, upwind flux



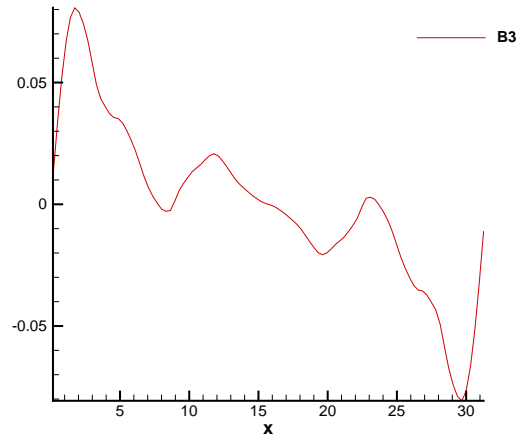
(c) Electric field, central flux



(d) Magnetic field, central flux



(e) Electric field, alternating flux



(f) Magnetic field, alternating flux

FIG. S10. Streaming Weibel instability with parameter choice 2 as in [1] ( $\delta = 1/6, v_{0,1} = 0.5, v_{0,2} = 0.1, k_0 = 0.2$ ). The mesh is  $100^3$  with piecewise quadratic polynomials. The electric and magnetic fields at  $T = 200$ .